Supporting Information

Fluorinated carbon nitride with hierarchical porous structure ameliorating PEO for high-voltage, high-rate solid lithium metal batteries†

Shuohan Liu,[a] Jieqing Shen,[a] Zhikai Wang,[a] Wensheng Tian,[b] Xiujun Han,[c] Zhixin Chen,[d] Hui Pan,*[a] Lei Wang,[a] Dongyu Bian,[a] Cheng Yang, *[be] Shenmin Zhu*[a]

[a]*State Key Laboratory of Metal Matrix Composites, School of Materials Science and Engineering, Shanghai Jiao Tong University, Shanghai, 200240, China*
[b]*State Key Laboratory of Space Power-Sources Technology, Shanghai Institute of Space Power-Sources, No. 2965, Dongchuan Road, Minhang District, Shanghai, 200245, China*
[c]*School of Materials Science and Engineering, Qilu University of Technology (Shandong Academy of Sciences), Jinan, Shandong Province, 250353, China*
[d]*School of Mechanical, Materials & Mechatronics Engineering, University of Wollongong, Wollongong, NSW, 2522, Australia*
[e]*School of Materials Science and Engineering, Harbin Institute of Technology, Harbin, Heilongjiang 150001, China*

* Corresponding authors.
E-mail: panhui115@sjtu.edu.cn (H. P.); yangcheng_811@sina.com (C. Y.); smzhu@sjtu.edu.cn (S. Z)

Supporting Information

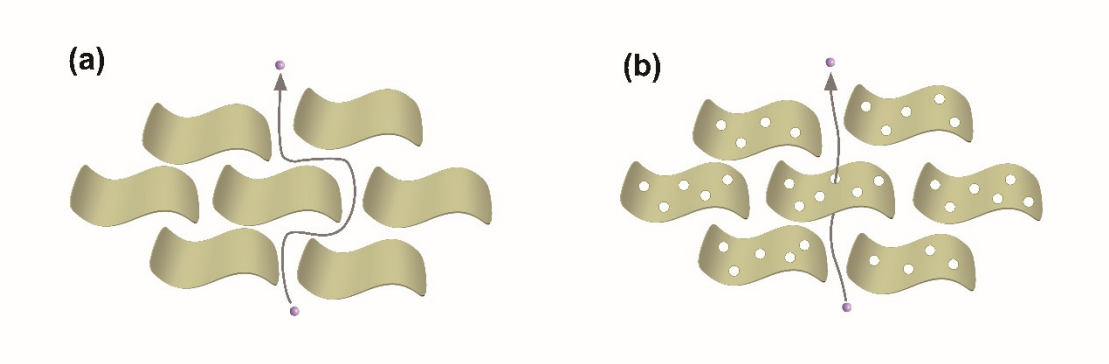

Fig. S1. (a) When two-dimensional nanosheets are used as electrolyte fillers, lithium ions need to be transported bypassing the nanosheets. (b) When porous nanosheets are used as electrolyte fillers, lithium ions can be transported through the porous and in as straight a line as possible, so the hierarchical porous FCN significantly shorten the transport distance of lithium ions.

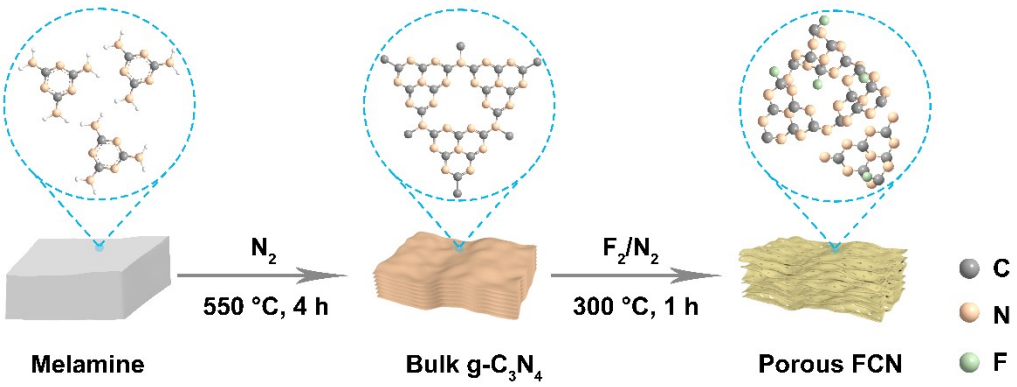

Fig. S2. Schematic synthesis process of FCN nanosheets.

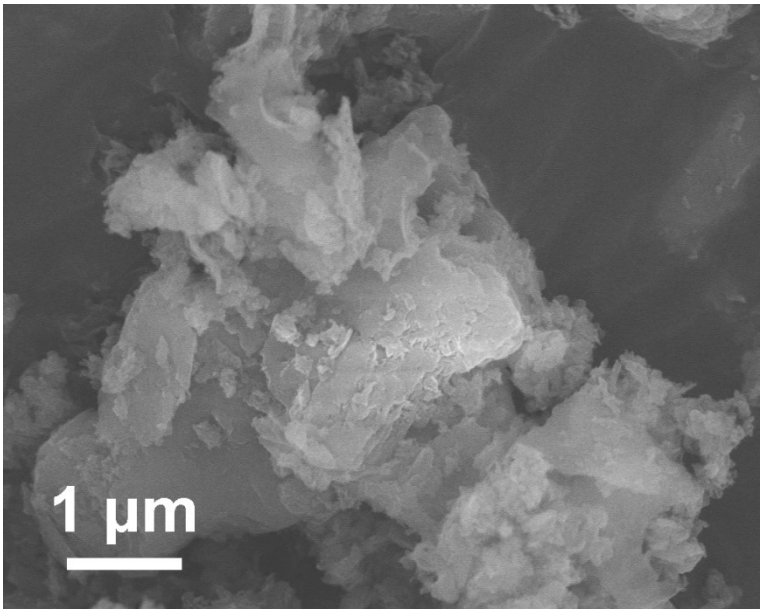

Fig. S3. SEM image of bulk g-C_3N_4.

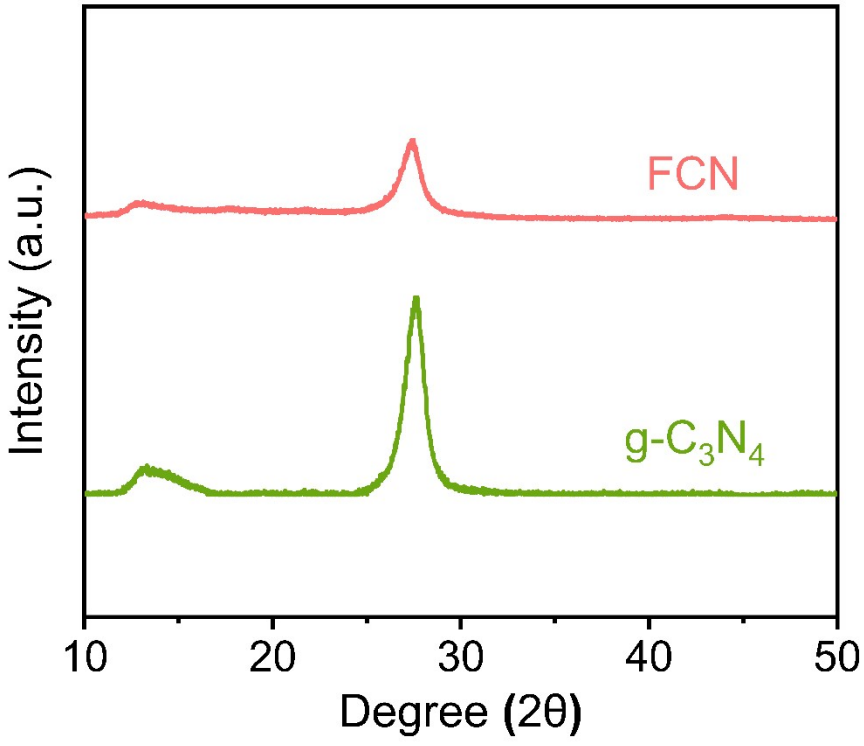

Fig. S4. XRD patterns of bulk g-C_3N_4 and FCN nanosheets.

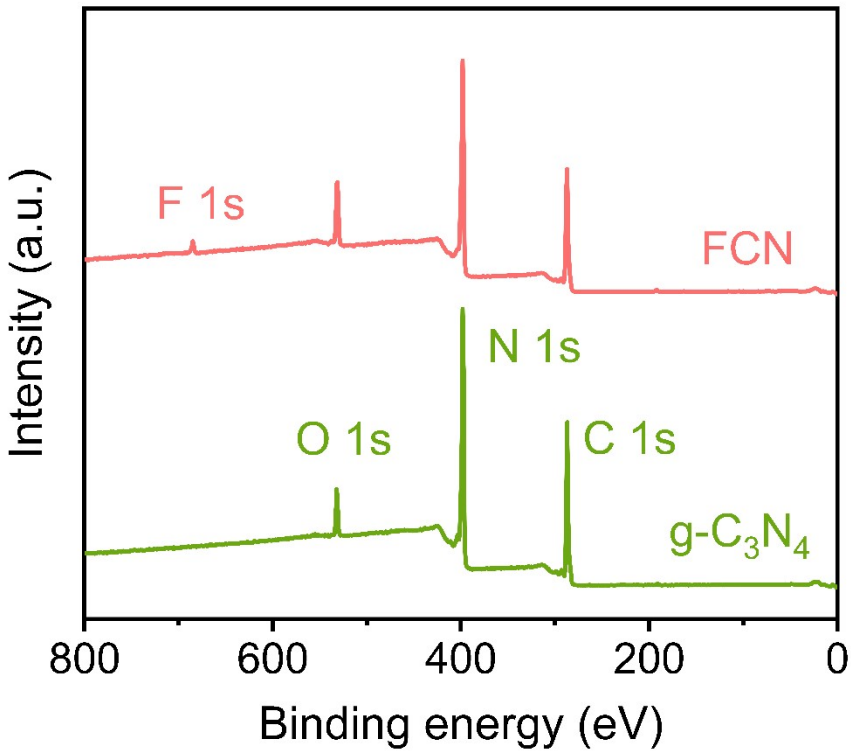

Fig. S5. XPS survey spectra of bulk g-C_3N_4 and FCN nanosheets.

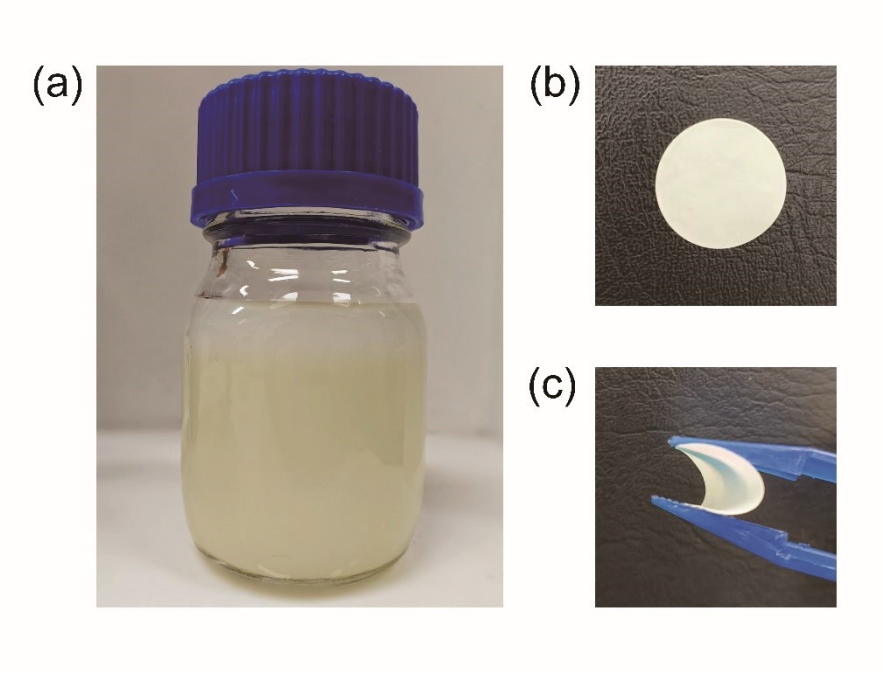

Fig. S6. (a) Photos of light-yellow solution containing FCN, LiTFSI and PEO after

resting for 7 days, as well as (b), (c) FCN reinforced composite polymer membrane.

Table S1. Characteristic parameters for PEO/LiTFSI and 0.1FCN-PEO/LiTFSI electrolytes, including melting enthalpy change (ΔH, J g^{-1}), relative PEO content (χ, %), and crystallinity (χ_c, %). χ_c is calculated from the equation $\chi_c = \left(\Delta H/\left(\chi \times \Delta H^*\right)\right) \times 100$, where ΔH^* (213.7 J g^{-1}) is the melting enthalpy change of completely crystallized PEO.

Abbreviation of sample	ΔH (J g^{-1})	Relative PEO content (χ, %)	Crystallinity (χ_c, %)
PEO/LiTFSI	47.31	71	31.2
0.1FCN-PEO/LiTFSI	31.59	66	22.4

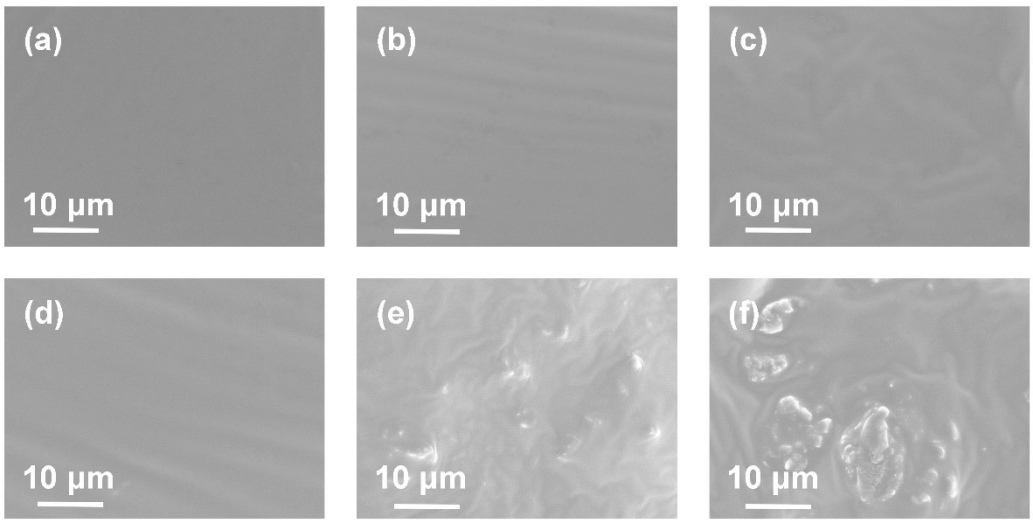

Fig. S7. Cross-sectional SEM images of PEO/LiTFSI electrolyte with (a) 0 wt.%, (b) 3 wt.%, (c) 5 wt.%, (d) 10 wt.%, (e) 15 wt.% and (f) 20 wt.% FCN.

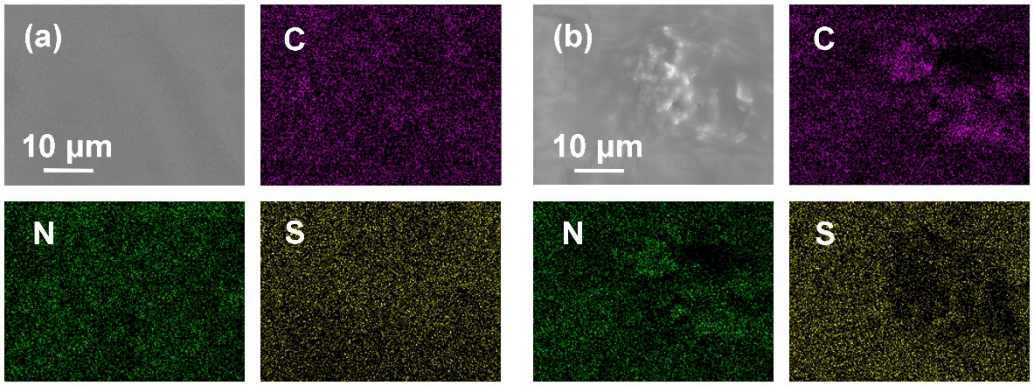

Fig. S8. EDS mappings of (a) 0.1FCN-PEO/LiTFSI and (b) 0.2FCN-PEO/LiTFSI for the elements of C, N and S.

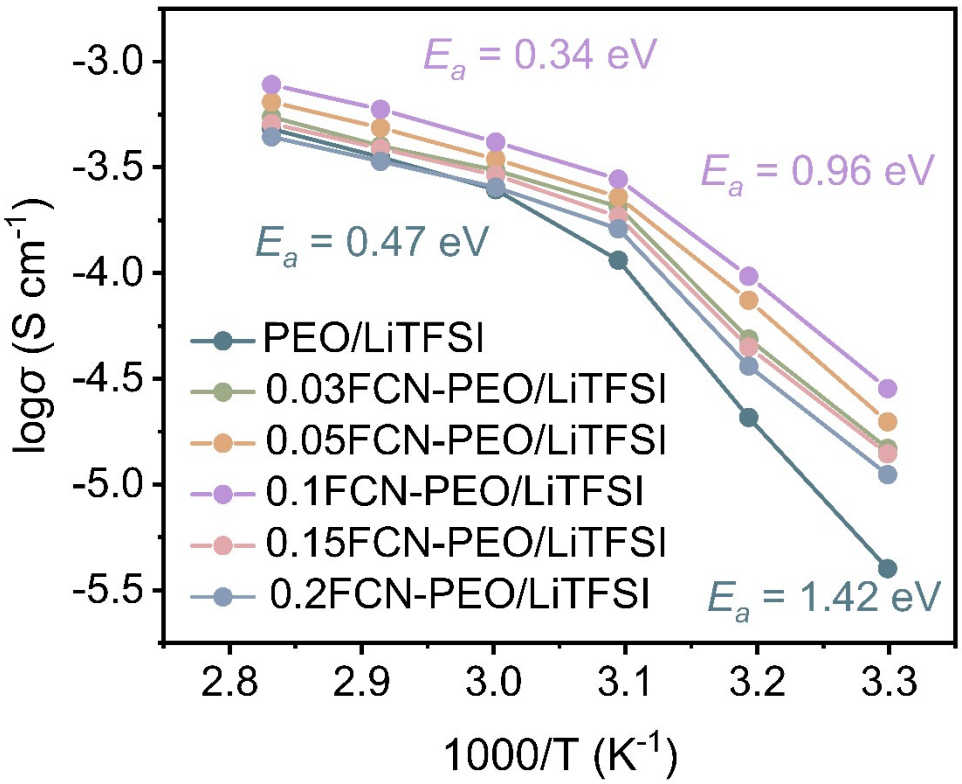

Fig. S9. Arrhenius plots for FCN-PEO/LiTFSI electrolytes with different amounts of FCN.

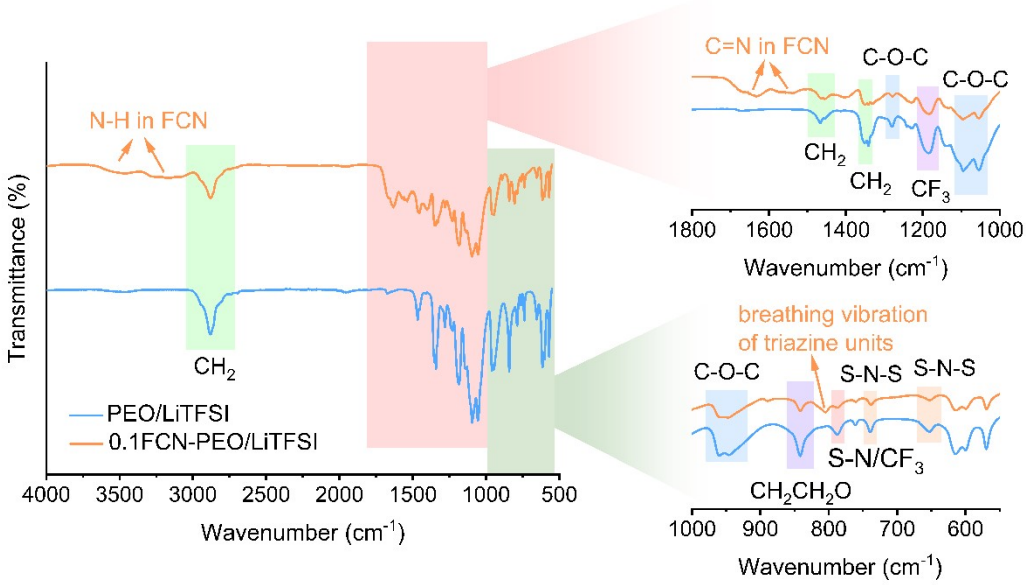

Fig. S10. FTIR spectra of PEO/LiTFSI and 0.1FCN-PEO/LiTFSI. The amplified spectra in the wavenumber ranges of 1000-1800 cm^{-1} and 550-1000 cm^{-1} are shown as insets on the right.

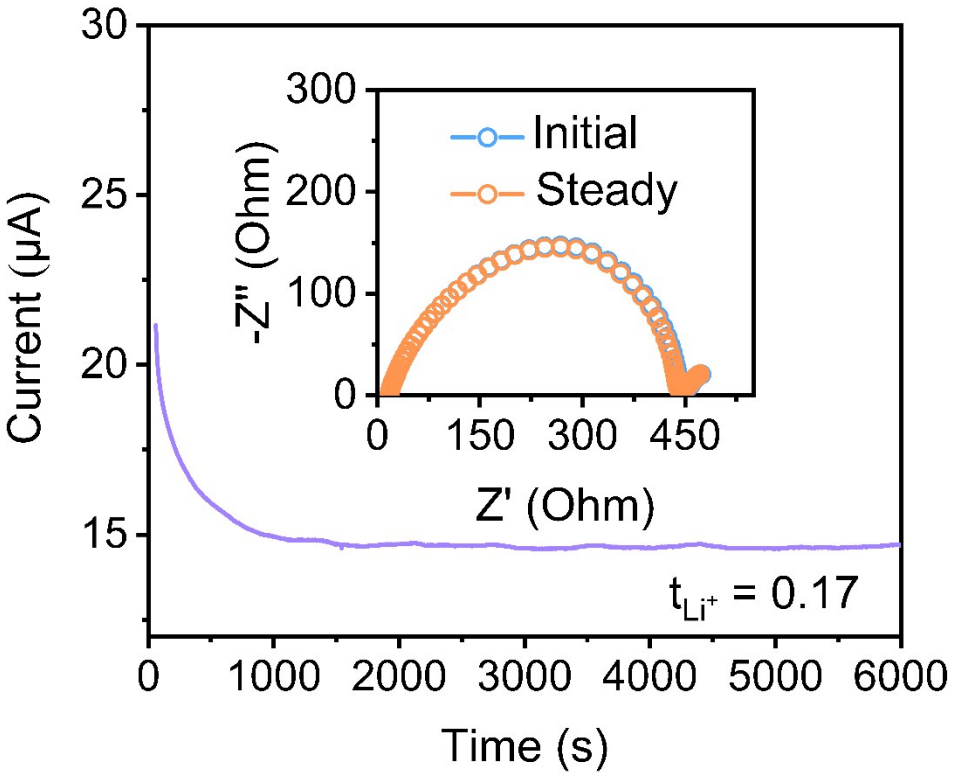

Fig. S11. Chronoamperometry curve of Li||PEO/LiTFSI||Li symmetric cell at a voltage bias of 10 mV for a duration time of 6000 s, inset: AC impedance spectra of Li||PEO/LiTFSI||Li cell before and after polarization at 60 °C.

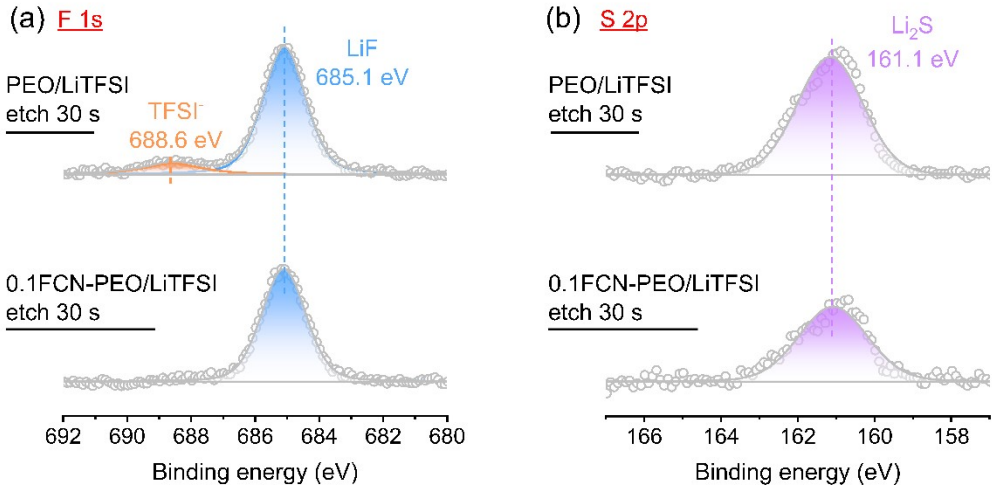

Fig. S12. *Ex situ* XPS measurements of lithium metal anode surface after cycling for both the PEO/LiTFSI and 0.1FCN-PEO/LiTFSI systems, with the signals of (a) F 1s and (b) S 2p.

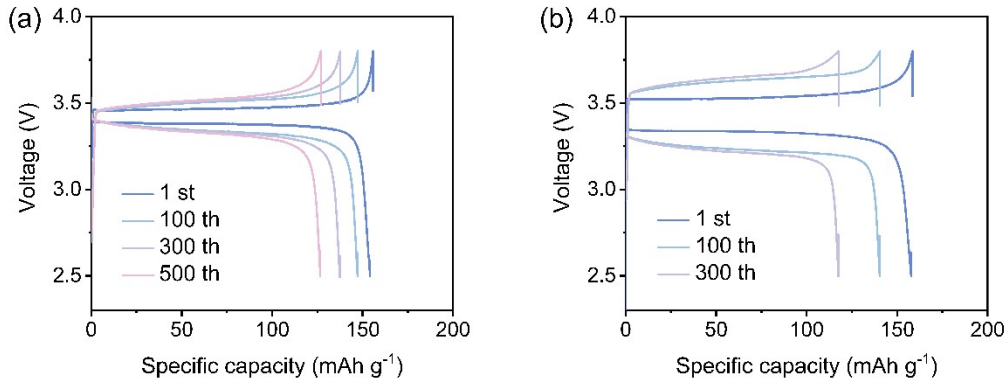

Fig. S13. Charge/discharge curves of (a) Li||0.1FCN-PEO/LiTFSI||LFP and (b) Li||PEO/LiTFSI||LFP cells at 1 C.

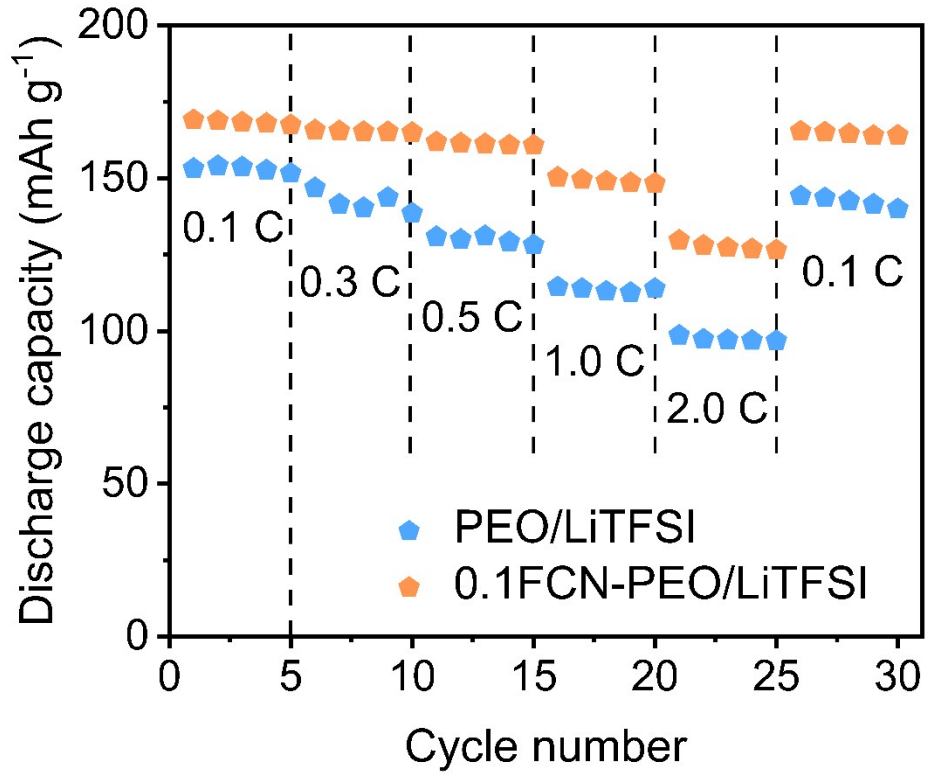

Fig. S14. Rate performance of LFP cells at 60 °C.

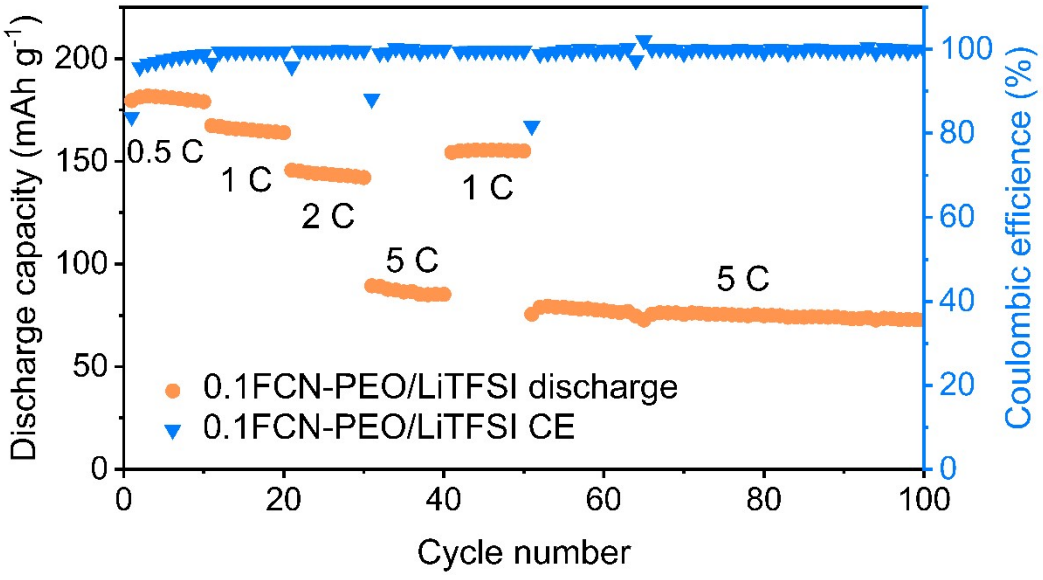

Fig. S15. Rate performance of Li||0.1FCN-PEO/LiTFSI||NCM523 cell.

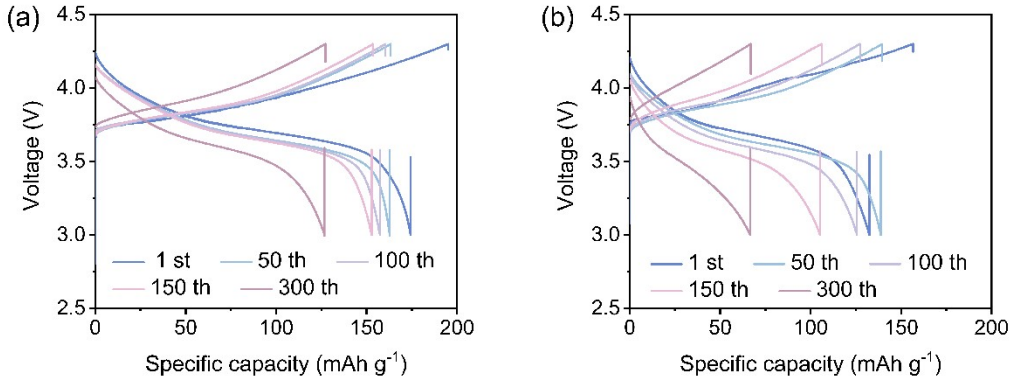

Fig. S16. Charge/discharge curves of (a) Li||0.1FCN-PEO/LiTFSI||NCM523 and (b) Li||PEO/LiTFSI||NCM523 cells at 1 C.

Table S2. The cycle performance of Li||NCM523 cells assembled by PEO-based electrolytes.

Electrolyte	Temperature (℃)	Current density	Initial capacity (mAh g^{-1})	Cycle number	Reversible capacity (mAh g^{-1})	Capacity retention	Ref.
PEO/LiTFSI/LiDGO	60	0.5 C	-	100	128	≈85.3 %	[1]
T-PEO-PT	40	0.2 C	110.9	75	-	≈78.9 %	[2]
EO–MA@LAGP	60	0.2 C	-	125	~100	≈61.0 %	[3]
PEO/NS-CD	45	0.2 C	-	100	138.3	≈74.7 %	[4]
PEO/$LiClO_4$/BE	50	0.2 C	-	100	145.1	≈82.9 %	[5]
LA–PEO–PAM-3-1-1	30	0.2 C	-	110	87	≈79.1 %	[6]
0.1FCN-PEO/LiTFSI	60	1 C	145.3	300	126.7	87.2 %	This work
0.1FCN-PEO/LiTFSI	60	2 C	137	150	120.3	87.8 %	This work

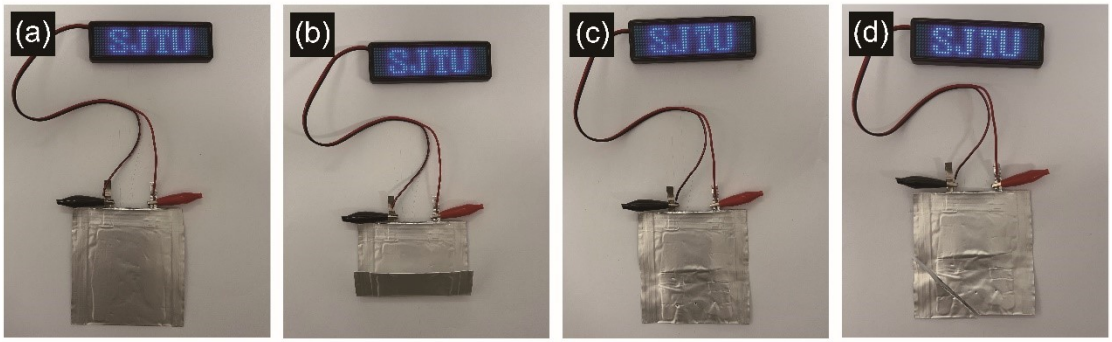

Fig. S17. Li||0.1FCN-PEO/LiTFSI||NCM523 pouch cells can (a) light up an LED while remaining operational under (b) bending, (c) puncturing, and (d) cutting situations.

Reference:

[1] Yang Z, Sun Z, Liu C, et al. Lithiated nanosheets hybridized solid polymer electrolyte to construct Li+ conduction highways for advanced all-solid-state lithium battery[J]. Journal of Power Sources, 2021, 484: 229287.

[2] Zheng J, Sun C, Wang Z, et al. Double Ionic–Electronic Transfer Interface Layers for All-Solid-State Lithium Batteries[J]. Angewandte Chemie International Edition, 2021, 60(34): 18448-18453.

[3] Liang Y, Chen N, Li F, et al. Melamine-Regulated Ceramic/Polymer Electrolyte Interface Promotes High Stability in Lithium-Metal Battery[J]. ACS Applied Materials & Interfaces, 2022, 14(42): 47822-47830.

[4] Xu L, Li J, Li L, et al. Carbon dots evoked Li ion dynamics for solid state battery[J]. Small, 2021, 17(39): 2102978.

[5] Xu L, Li J, Xiang Y, et al. Few-layer bismuthene enabled solid-state Li batteries[J].

Energy Storage Materials, 2022, 52: 655-663.

[6] Wen X, Zeng Q, Guan J, et al. 3D structural lithium alginate-based gel polymer electrolytes with superior high-rate long cycling performance for high-energy lithium metal batteries[J]. Journal of Materials Chemistry A, 2022, 10(2): 707-718.